Supporting Information

An easily-synthesized AIE luminogen for lipid droplets-specific super-resolution imaging and two-photon imaging

Yanzi Xu,[a,‡] Haoke Zhang,[b,‡] Ning Zhang,[a,‡] Ruohan Xu,[a] Zhi Wang,[a] Yu Zhou,[a,c] Qifei Shen,[a] Dongfeng Dang,[a,] Lingjie Meng,[a,c,*] Ben Zhong Tang [b,*]*

[a] School of Chemistry, MOE Key Laboratory for Non-equilibrium Synthesis and Modulation of Condensed Matter, Xi'an Key Laboratory of Sustainable Energy Material Chemistry, Xi'an Jiao Tong University, Xi'an 710049, P. R. China.

[b] Department of Chemistry, The Hong Kong University of Science and Technology, Hong Kong, P. R. China.

[c] Instrumental analysis center, Xi'an Jiao Tong University, Xi'an, 710049, P. R. China.

E-mails: dongfengdang@xjtu.edu.cn, menglingjie@xjtu.edu.cn

tangbenz@ust.hk

‡ Y. Xu, H. Zhang and N. Zhang contributed equally to this manuscript.

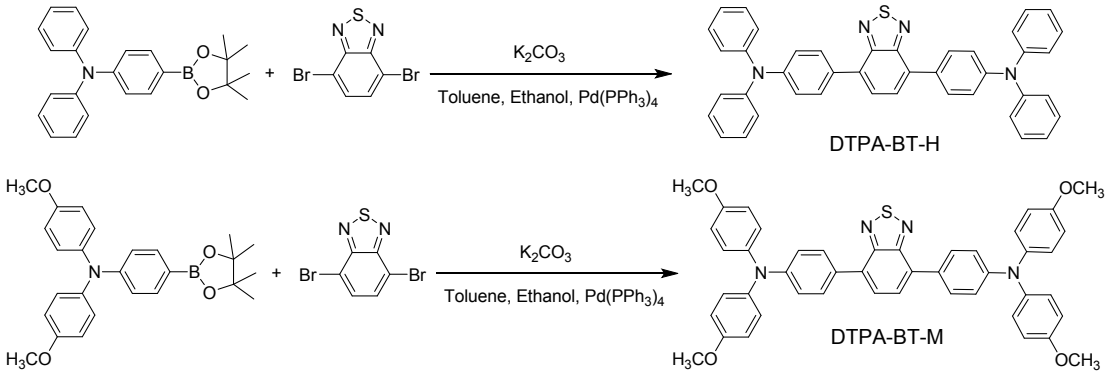

Scheme S1. Synthetic routes to DTPA-BT-H and DTPA-BT-M.

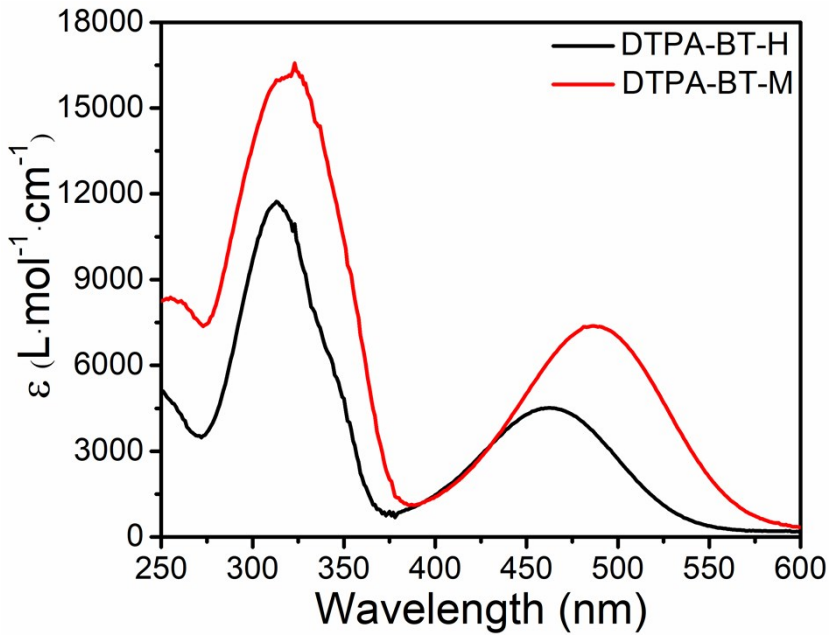

Figure S1. UV-Vis absorption spectra and molar absorption coefficient of DTPA-BT-H and DTPA-BT-M in dilute THF solution ([*c*]=1×10^{-5} mol/L).

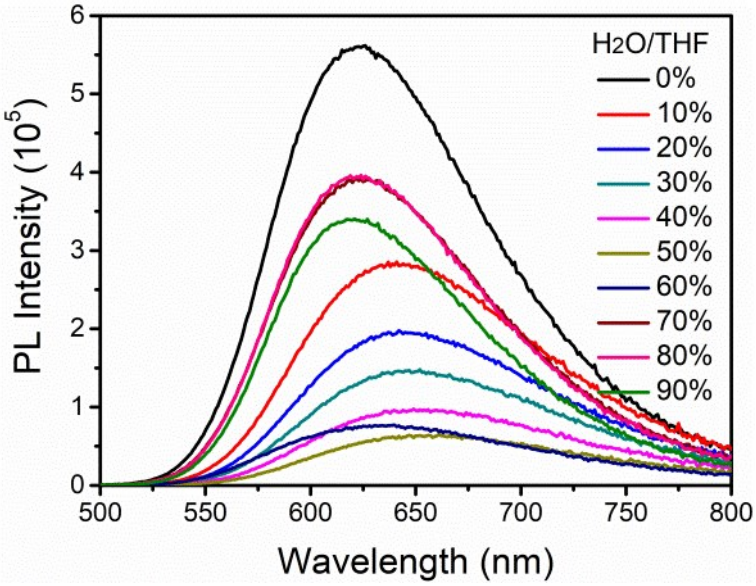

Figure S2. PL spectra of DTPA-BT-H in a THF/water mixture with different water fraction ([*c*]=1×10^{-5} mol/L).

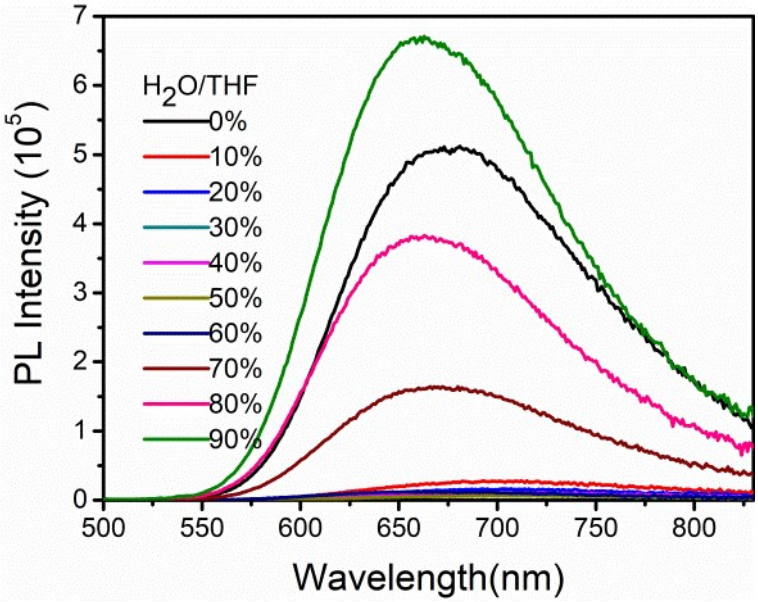

Figure S3. PL spectra of DTPA-BT-M in a THF/water mixture with different water fraction ([*c*]=1×10^{-5} mol/L).

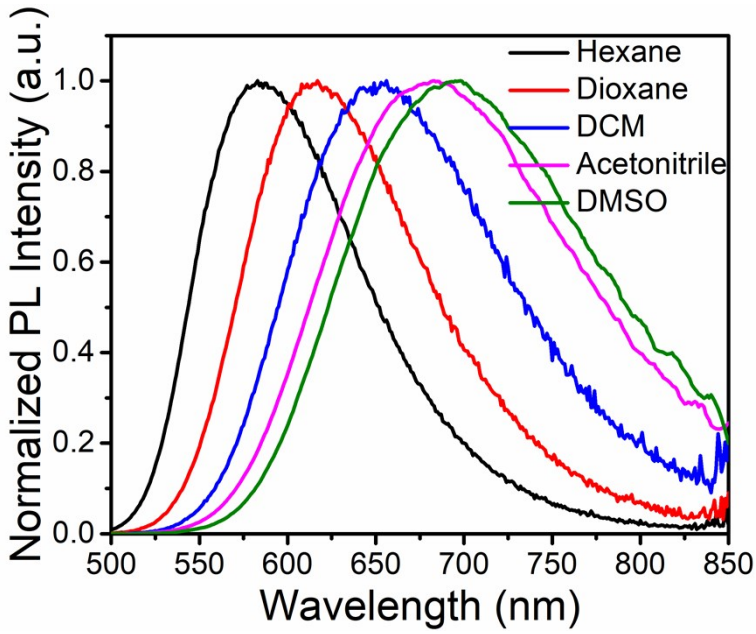

Figure S4. Normalized PL spectra of DTPA-BT-H in solvents with varied polarities.

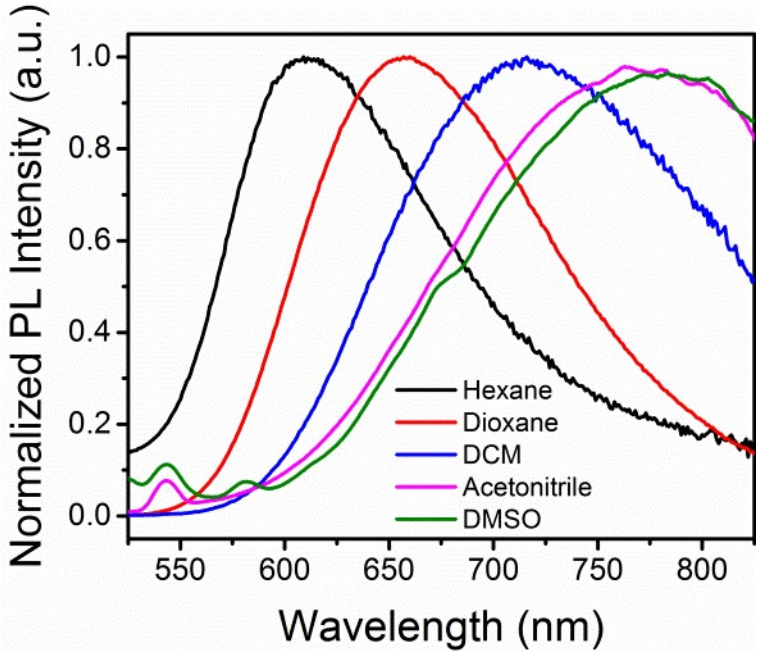

Figure S5. Normalized PL spectra of DTPA-BT-M in solvents with varied polarities.

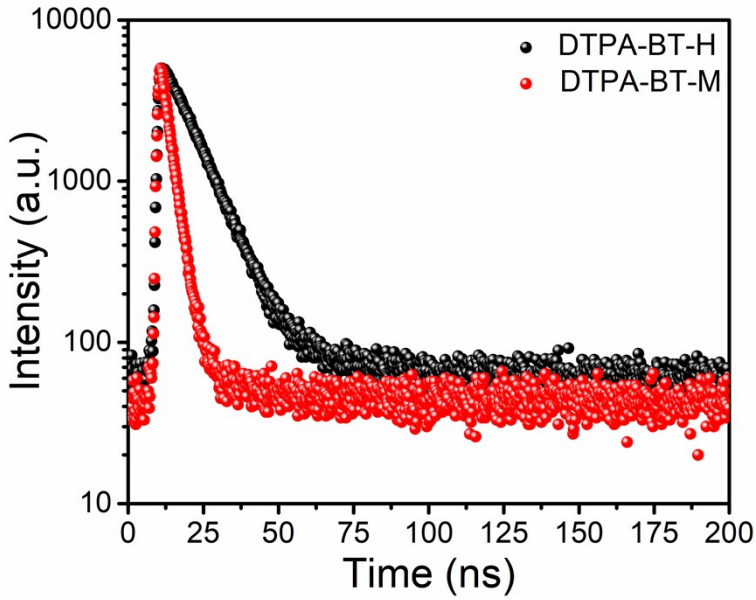

Figure S6. Transient decay spectra of DTPA-BT-H and DTPA-BT-M in dilute THF solution ([*c*]=1×10^{-5} mol/L).

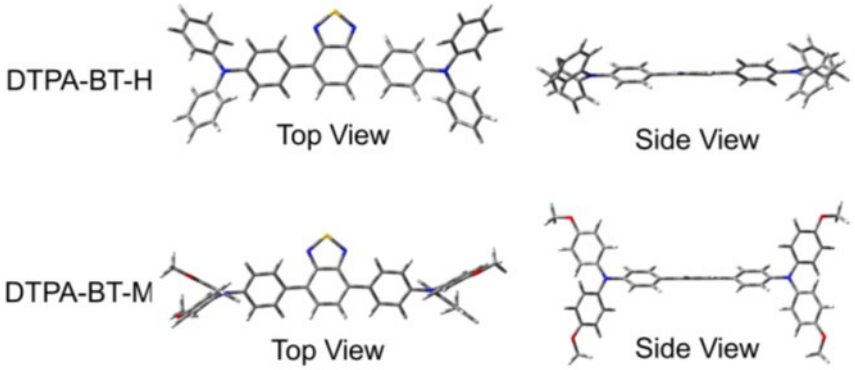

Figure S7. The calculated geometries of DTPA-BT-H and DTPA-BT-M in excited states (including top view and side view).

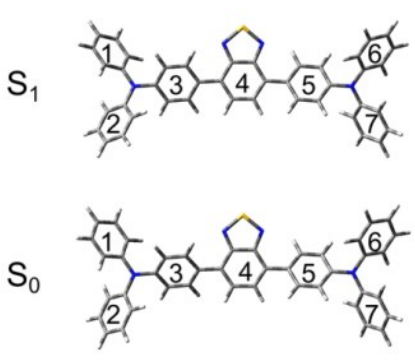

Degree (°)	DTPA-BT-H	
	S_0	S_1
1-N	42	41
2-N	45	40
3-N	38	39
3-4	35	23
4-5	35	23
5-N	38	39
6-N	45	41
7-N	42	40

Figure S8. The conformational change of DTPA-BT-H from ground state (S_0) to excited state (S_1).

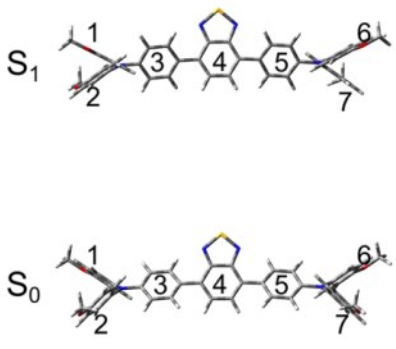

Degree (°)	DTPA-BT-M	
	S_0	S_1
1-N	47	36
2-N	48	36
3-N	32	50
3-4	35	27
4-5	35	27
5-N	32	49
6-N	45	36
7-N	48	36

Figure S9. The conformational change of DTPA-BT-M from ground state (S_0) to excited state (S_1).

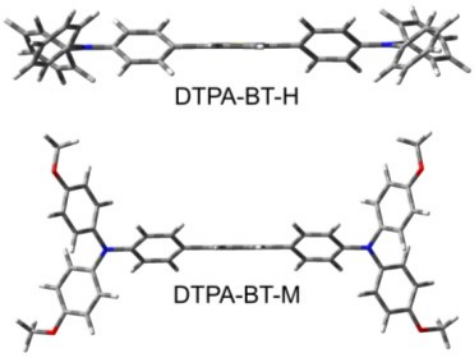

Figure S10. The single crystal structure of DTPA-BT-H and DTPA-BT-M in side view.

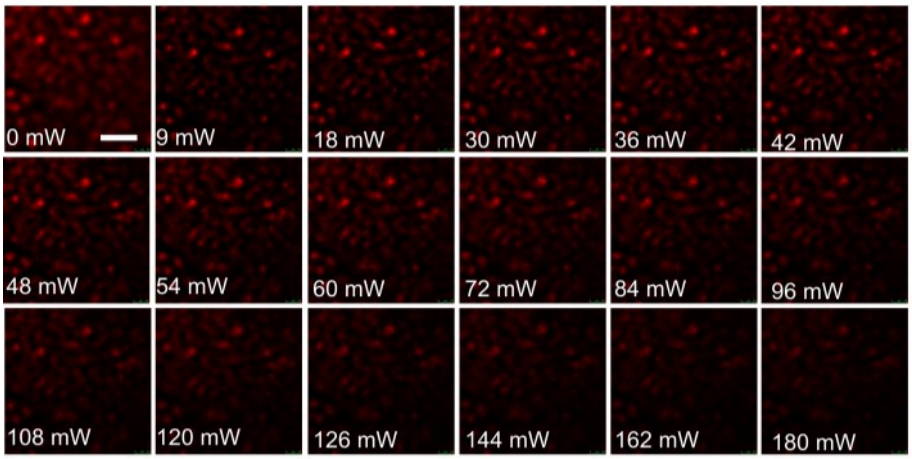

Figure S11. Power-dependent fluorescent images for DTPA-BT-H on AAO mask under the irradiation of STED beam (Scale bar = 2 μm).

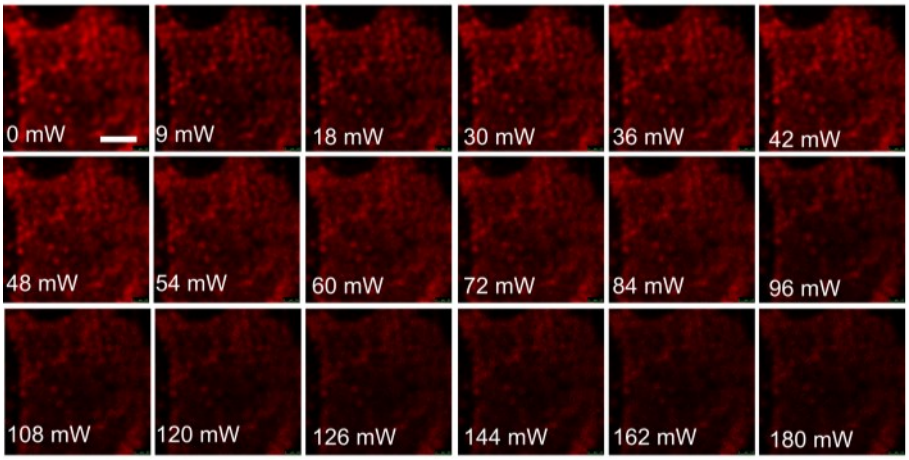

Figure S12. Power-dependent fluorescent images for DTPA-BT-M on AAO mask under the irradiation of STED beam (Scale bar = 2 μm).

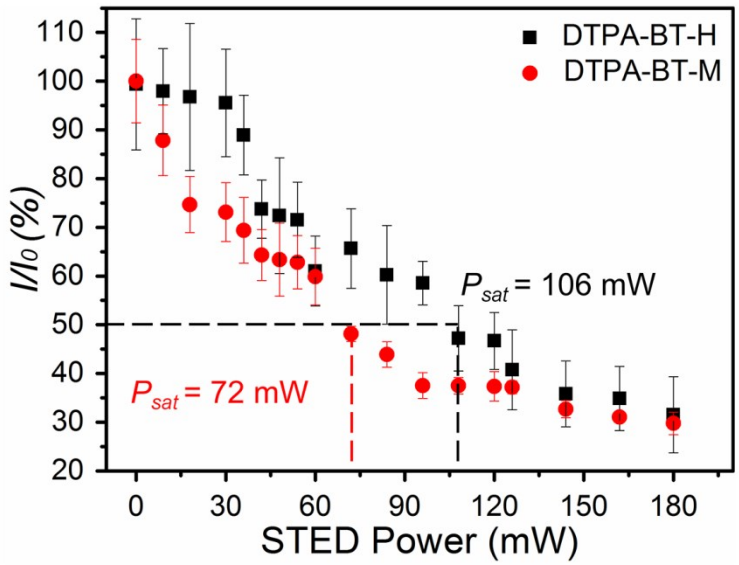

Figure S13. Plots of relative fluorescence intensity (I/I_0) for DTPA-BT-H and DTPA-BT-M on AAO mask under different STED power.

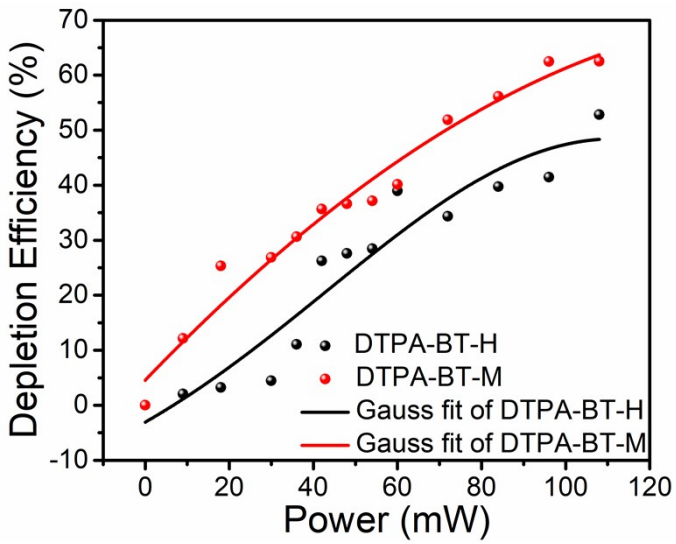

Figure S14. The fitting curve for depletion efficiency of DTPA-BT-H and DTPA-BT-M under various powers in STED nanoscopy.

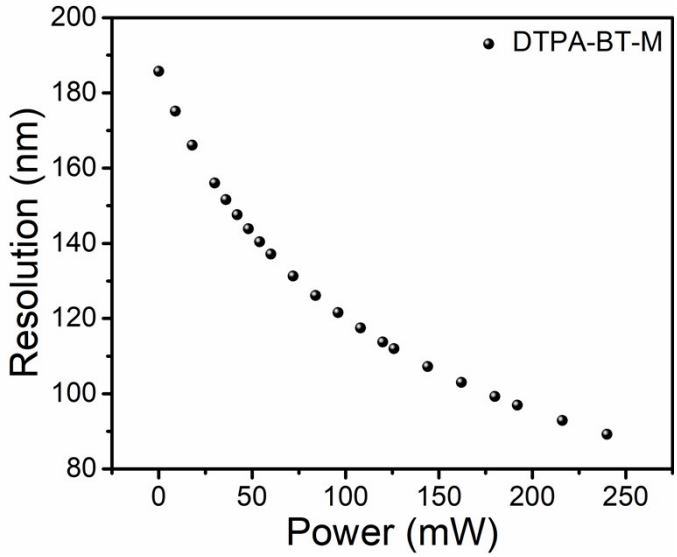

Figure S15. The calculated resolution for DTPA-BT-M under various STED power.

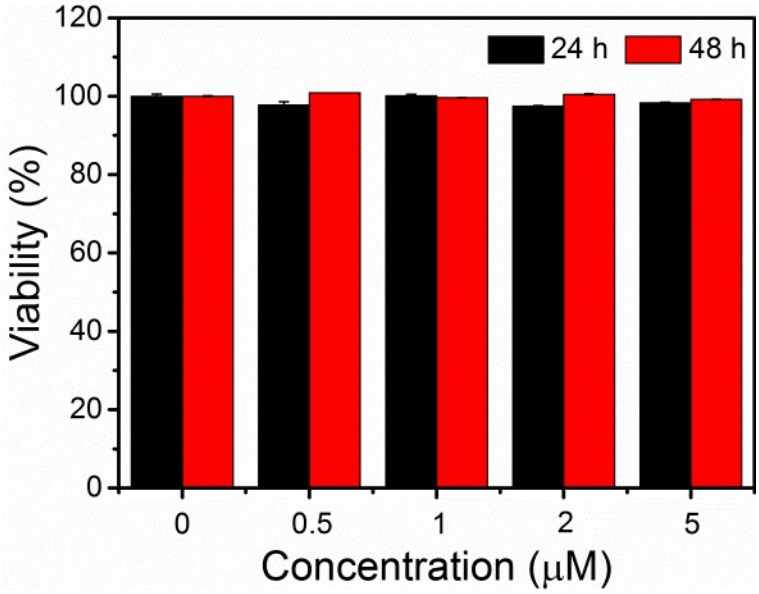

Figure S16. The viability of LO_2 cells after incubated with DTPA-BT-M for 24 h and 48 h under different concentration.

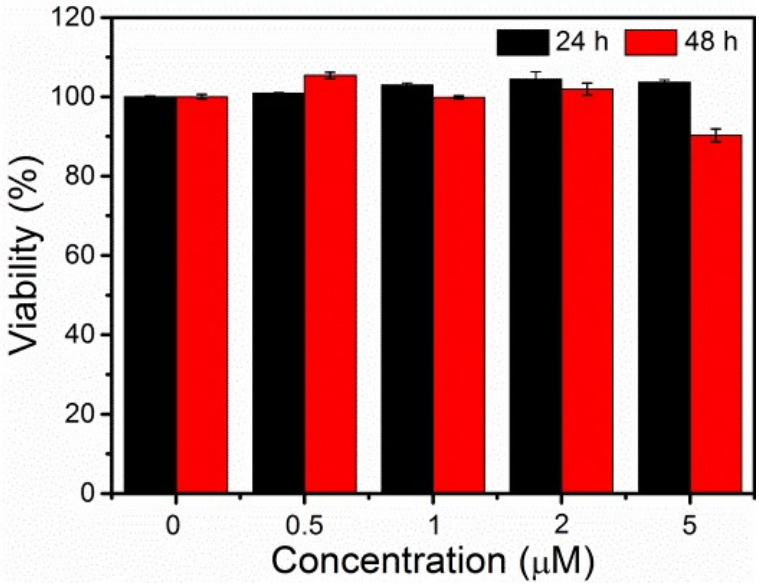

Figure S17. The viability of HeLa cells after incubated with DTPA-BT-M for 24 h and 48 h under different concentration.

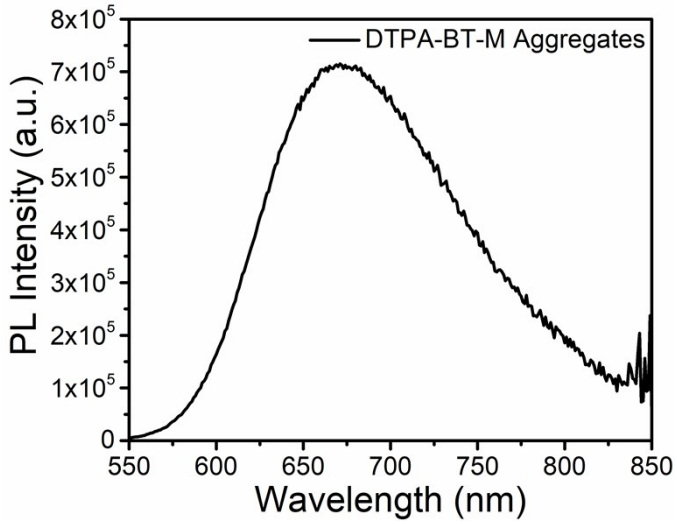

Figure S18. The PL spectra of DTPA-BT-M in DMSO and PBS solution for cell cultures.

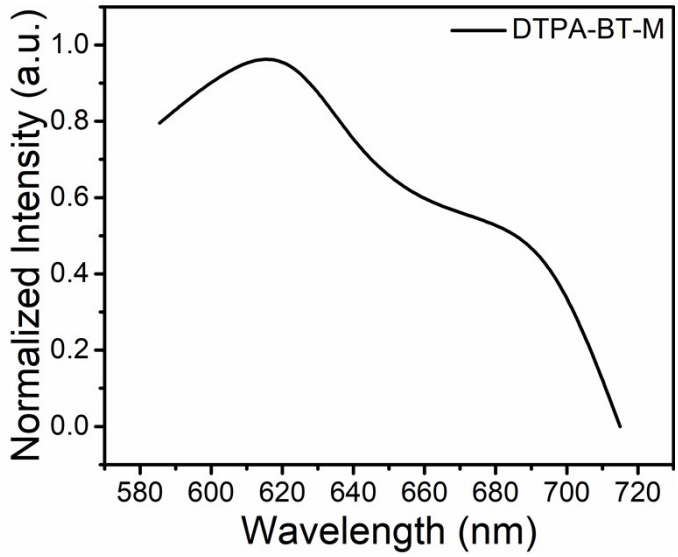

Figure S19. The PL spectra of DTPA-BT-M in HeLa cells.

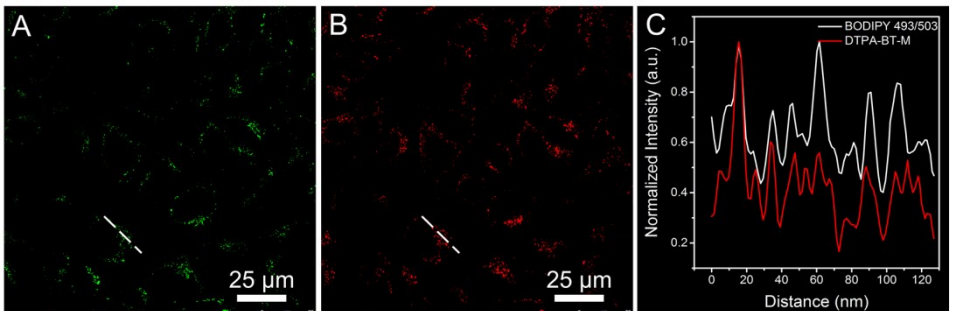

Figure S20. Confocal images of HeLa cells stained with BODIPY 493/503 (A), DTPA-BT-M (B) and their corresponding co-location profile by A and B (C).

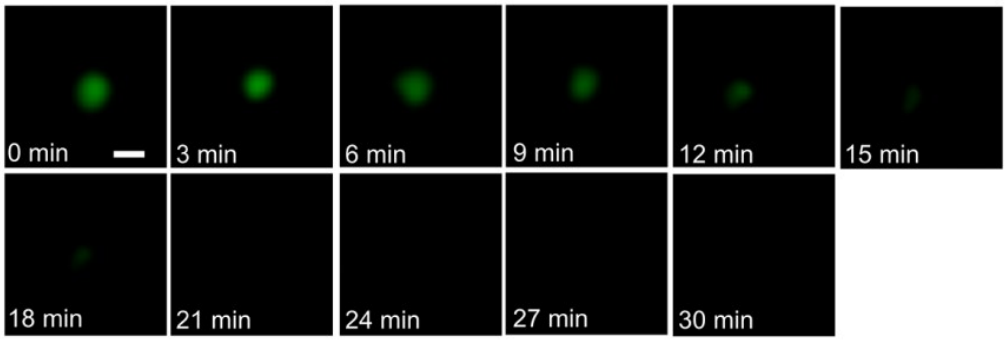

Figure S21. Time-dependent fluorescent images for BODIPY 493/503 stained HeLa cells under the irradiation of STED beam (Scale bar = 300 nm).

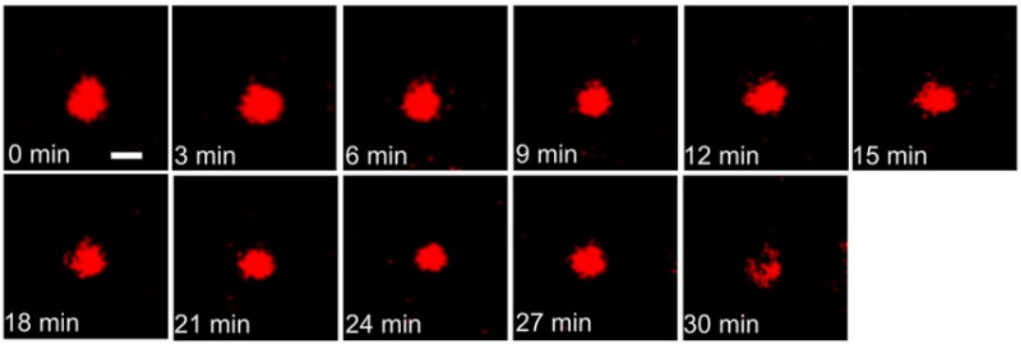

Figure S22. Time-dependent fluorescent images for DTPA-BT-M stained HeLa cells under the irradiation of STED beam (Scale bar = 300 nm).

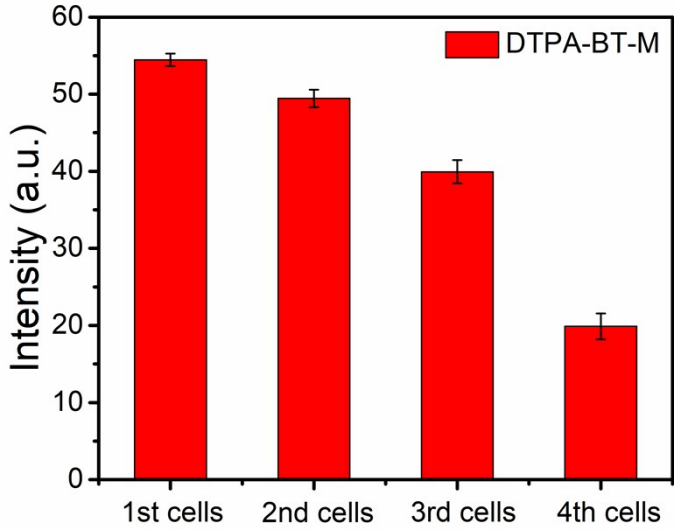

Figure S23. Fluorescent intensity for DTPA-BT-M-stained cells over various generations.

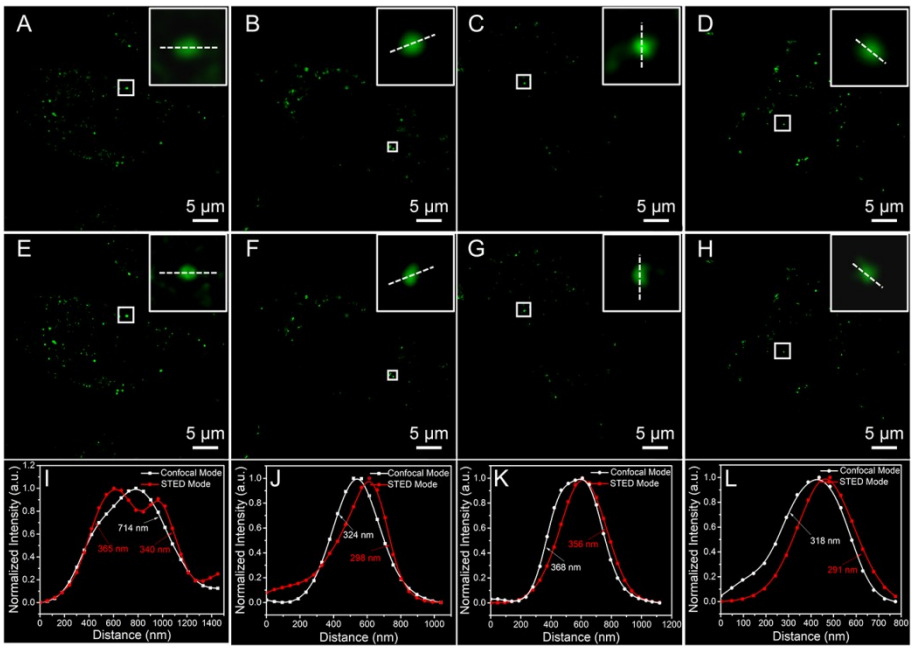

Figure S24. Fluorescence images by CLSMs (A-D) and STED nanoscopy (E-H) in long-term cellular tracking by using BODIPY 493/503; Fluorescence intensity along the white line in captured images by CLSMs and STED nanoscopy, and their corresponding FWMH values (I-L).

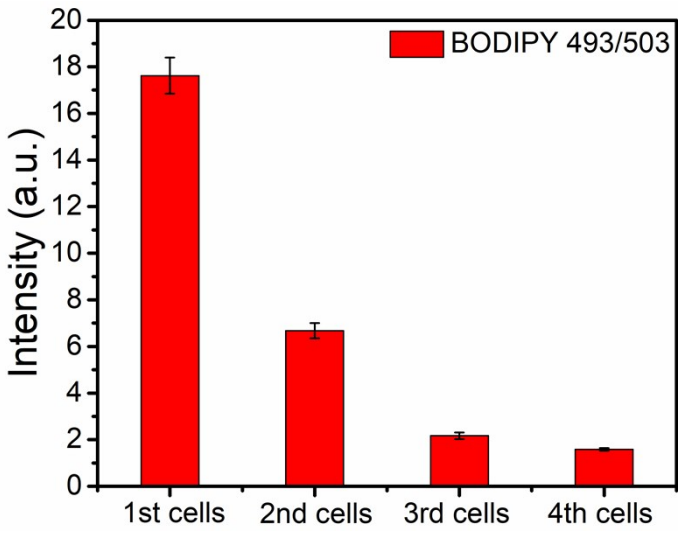

Figure S25. Fluorescent intensity for BODIPY 493/503-stained cells over various generations.

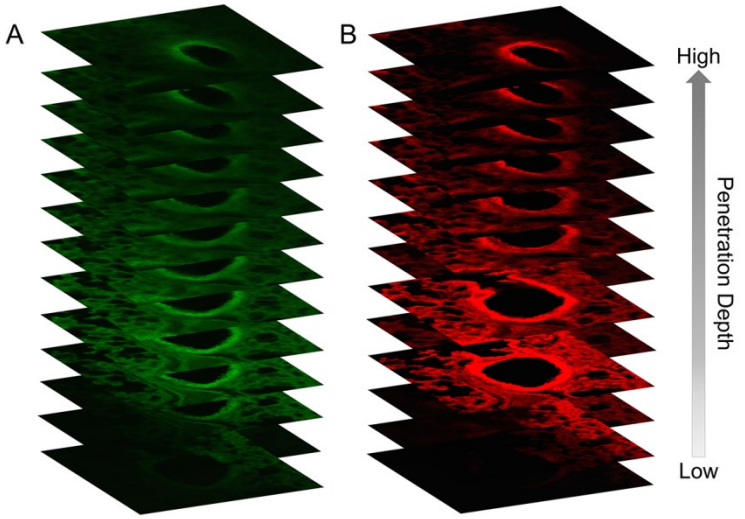

Figure S26. Fluorescence images of DTPA-BT-M stained lung tissue in one-photon mode (A) and two-photon mode (B) at different penetration depth.

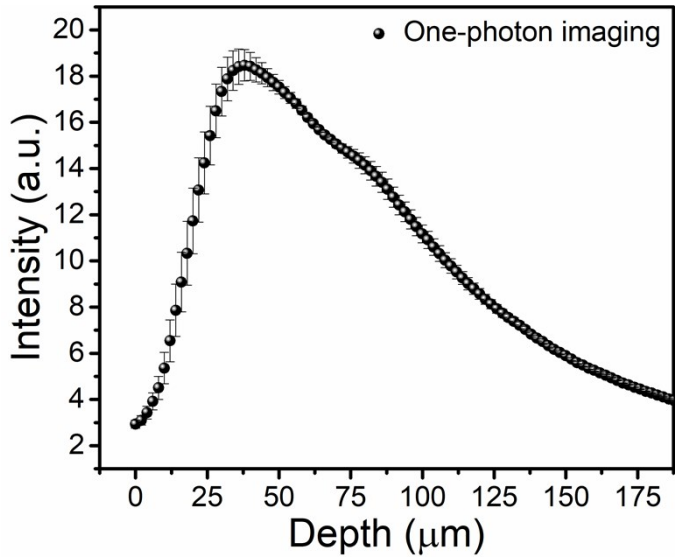

Figure S27. The fluorescent intensity curve for DTPA-BT-M at various penetration depths in one-photon imaging.

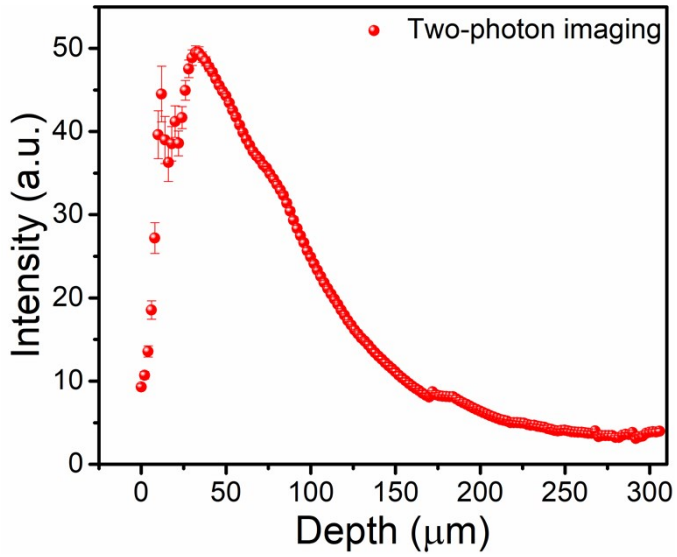

Figure S28. The fluorescent intensity curve for DTPA-BT-M at various penetration depths in two-photon imaging.

Table S1. The δ_{2PA} of typical AIEgens for two-photon fluorescence microscopy.

Sample	Ex	δ_{2PA}
TBP-*b*-TPA [a]	1040 nm	207±7 GM
CDPP-4SO3 [b]	820 nm	162 GM
BTPETQ dots [c]	1200 nm	7.63×10^4 GM
TP [d]	840 nm	265 MG
TQ-BPN [e]	1300 nm	1.22×10^3 GM
DTPA-BT-M [f]	840 nm	1581 GM

[a] Angew. Chem. Int. Ed. 2020, 59, 12822; [b] Adv. Funct. Mater. 2020, 30, 1909268; [c] Adv. Mater. 2019, 31, 1904447; [d] Nano Res. 2019, 12, 1703; [e] ACS Nano 2018, 12, 7936; [f] our work.

NMR and MS spectra

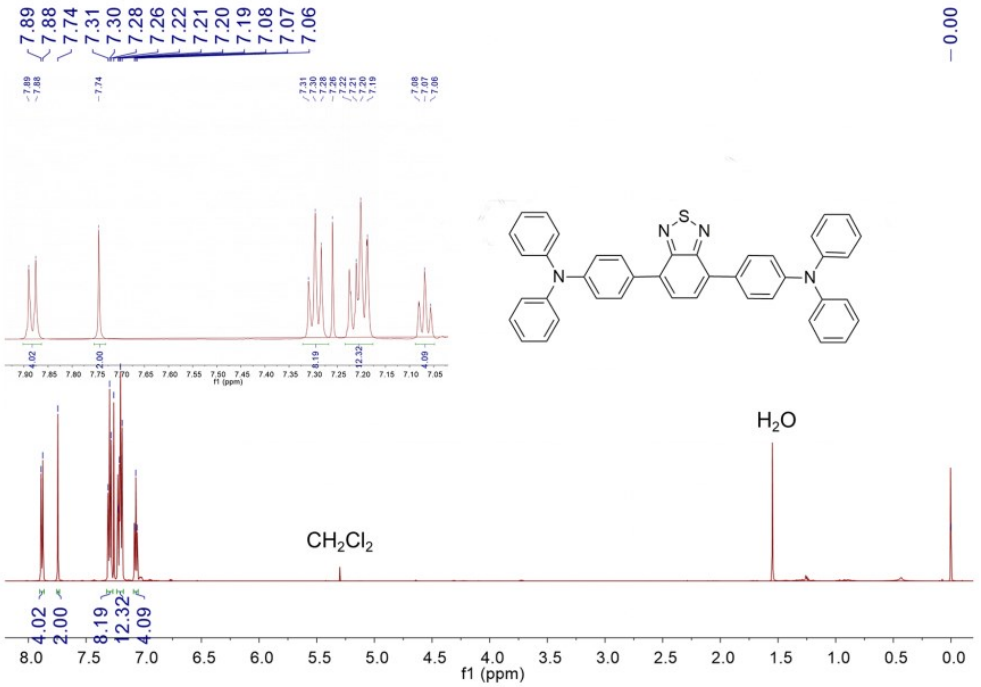

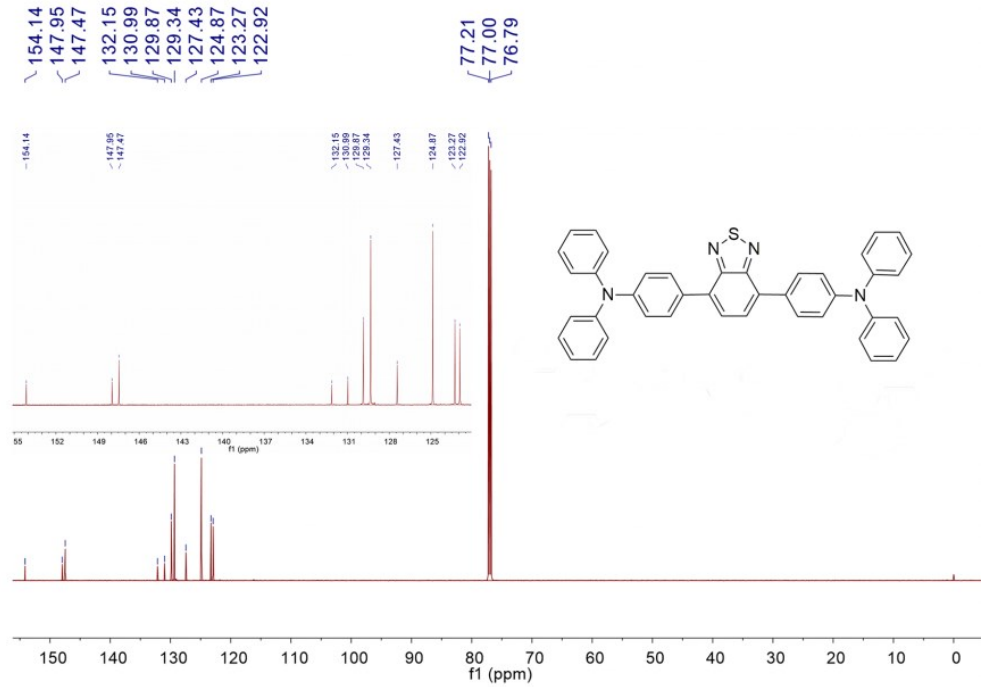

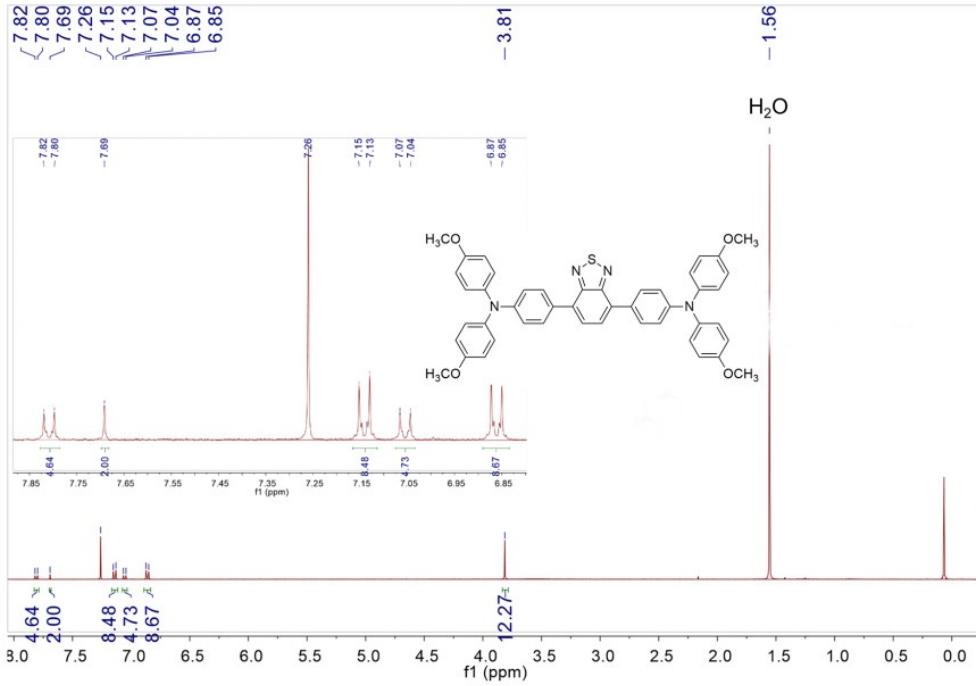
7.82
7.80
7.69
7.26
7.15
7.13
7.07
7.04
6.87
6.85
3.81
1.56
H2O
4.64
2.00
8.48
4.73
8.67
12.27
f1 (ppm)

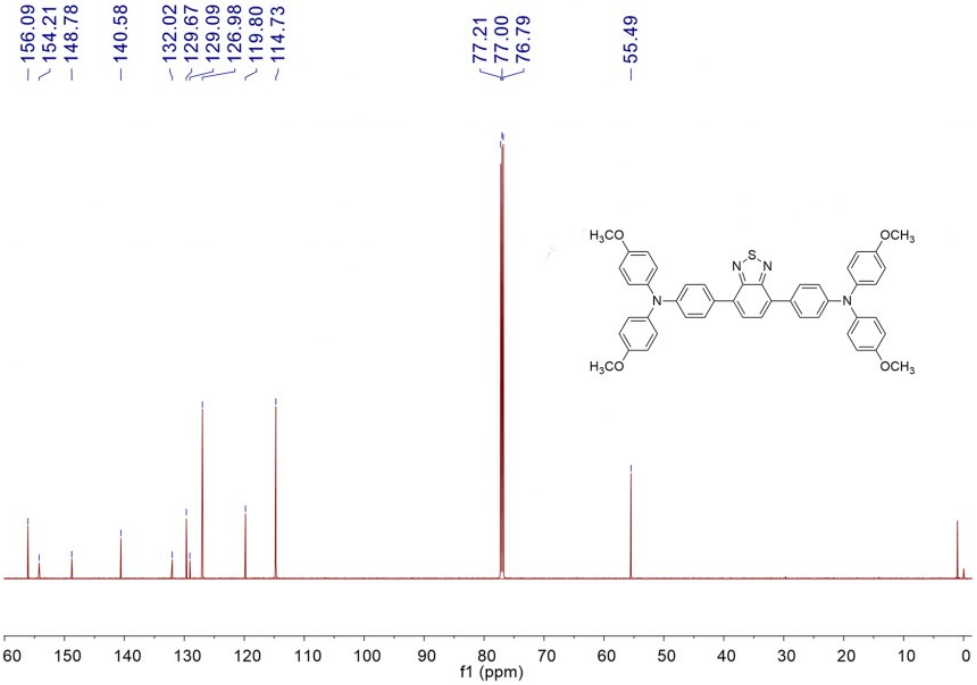
156.09
154.21
148.78
140.58
132.02
129.67
129.09
126.98
119.80
114.73
77.21
77.00
76.79
55.49
f1 (ppm)

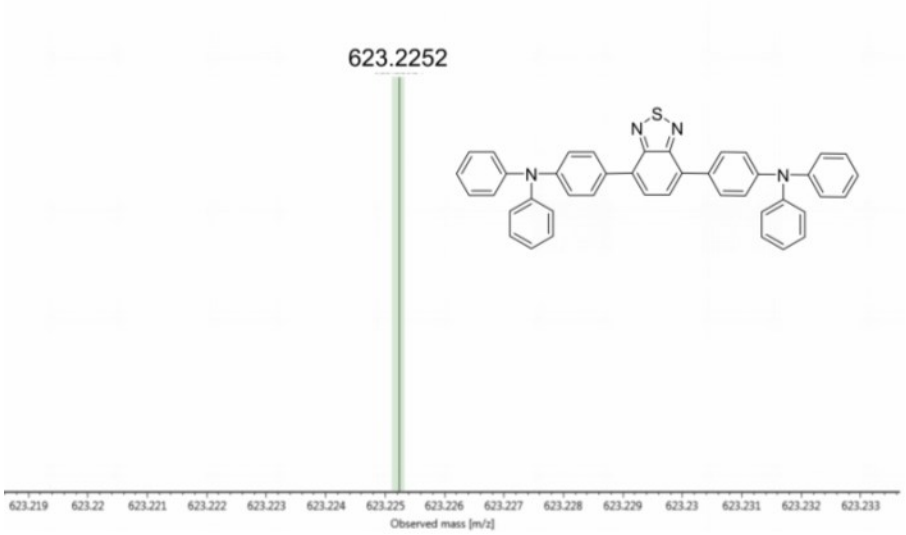
623.2252
623.219
623.22
623.221
623.222
623.223
623.224
623.225
623.226
623.227
623.228
623.229
623.23
623.231
623.232
623.233
Observed mass [m/z]

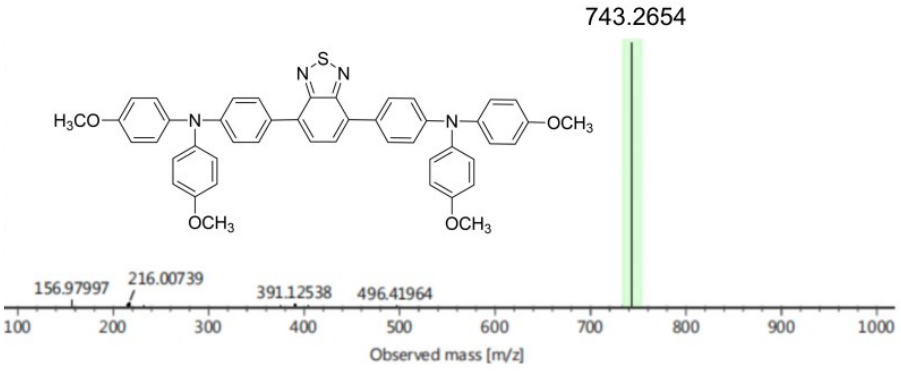
743.2654
156.97997
216.00739
391.12538
496.41964
100
200
300
400
500
600
700
800
900
1000
Observed mass [m/z]